JCTC Journal of Chemical Theory and Computation

pubs.acs.org/JCTC Article

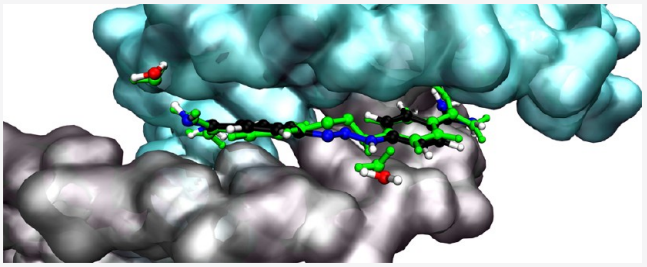
Relaxation Dynamics of the Triazene Compound Berenil in DNA-Minor-Groove Confinement after Photoexcitation

Alireza Marefat Khah,* Peter Reinholdt, Patrick Nuernberger, Jacob Kongsted, and Christof Hättig

Cite This: J. Chem. Theory Comput. 2020, 16, 5203−5211 Read Online

ACCESS | Metrics & More | Article Recommendations | Supporting Information

ABSTRACT: The effects of biomolecular embedding on the photoinduced relaxation process of the DNA-minor-groove binder berenil, diminazene aceturate, are studied with quantum mechanics/molecular mechanics, QM/MM, calculations that employ the algebraic diagrammatic construction through second-order, ADC(2), for the quantum mechanical part and an atomistic polarizable embedding for the classical part. The lowest singlet excitation to the S_1 state is a bright transition with a $\pi\pi^*$ character and a perichromatic red shift, due to the interactions with the solvent and DNA. The excited-state relaxation pathway is a two-step mechanism, an N═N azo-bond stretch followed by a volume-conserving bicycle-pedal twist. The DNA confinement and the coupling to solvent molecules via hydrogen bonds lead, for the excited-state relaxation process, only to small deviations from the ideal bicycle-pedal relaxation. Because of its volume-conserving character, the S_1 excited-state relaxation proceeds almost unhindered, even in a fully rigid minor-groove confinement. With a fully frozen DNA minor groove and solvent, the energy gap for deexcitation from S_1 to the ground state increased to 2.0 eV compared to 0.16 eV in aqueous solution. When the relaxation of the first solvation shell is included, the relaxation process on the S_1 potential energy surface proceeds to a region on the potential energy surface, where only a small gap to the ground-state potential energy surface remains, 0.43 eV. These results show that the solvent relaxation has a significant effect in controlling the energy gap between the ground and S_1 electronically excited states, which explains the experimental observations of the fluorescence characteristics of berenil in DNA confinement.



Downloaded via BOCHUM LIBRARIES on August 27, 2020 at 09:44:03 (UTC).
See https://pubs.acs.org/sharingguidelines for options on how to legitimately share published articles.

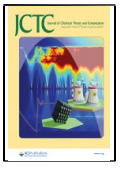
1. INTRODUCTION

Light-induced trans−cis isomerization processes of many organic chromophores around a chain of conjugated π-bonds involve torsions around a π-bond to diminish the unfavorable antibonding interactions in the π^* orbital that is occupied in a $\pi\pi^*$ electronic excitation. The torsion can lead to large amplitude motions that are hindered in (bio)molecular confinements and viscous solvents so that in these environments the relaxation processes are significantly delayed relative to nonviscous solvents or the gas phase.[1] In particular, for chains with several conjugated bonds, there are, besides simple rotations, also different volume-conserving mechanisms with spatially localized nuclear motions conceivable, which are less sensitive to confinement and solvent viscosity. Known examples exhibiting mechanisms beyond rotation include azobenzenes,[2−9] green fluorescent proteins,[10] the photoactive yellow protein,[11,12] rhodopsin[13] and mutants,[14] and others. The understanding of these mechanisms is, thus, important for many applications.

Some of the volume-conserving motions consist of synchronous multiple torsional motions.[15] For instance, the Hula-twist[16] and the bicycle-pedal rotation[13] comprise synchronous rotations around two adjacent or conjugated bonds,[15] respectively, while the double twist[4] and folding table[17] mechanisms incorporate synchronous rotations of three adjacent or conjugated bonds, respectively. However, a weak response to changes in viscosity and a volume-conserving relaxation mechanism does not mean that relaxation after photoexcitation is completely insensitive to the environment. Recently, Jung et al. showed that the bicycle-pedal type photoisomerization mechanism of the photoactive yellow protein could be controlled by mutating the contacting protein residues.[11] Moreover, the polarity of the environment, which has a nonisotropic effect in the case of biomolecular embedding and DNA confinement, can influence relaxation mechanisms even in volume-conserving cases.[10,18−20]

Berenil, or diminazene aceturate, is a DNA-minor-groove binder.[21−23a] In a recent study, some of us showed with *ab initio* calculations[24] that in solution and under thermodynamically equilibrated conditions at T = 298 K, the *E-azo,s-trans* (ET) conformer is the most stable and dominant conformer of berenil, Figure 1. Also, the UV/Vis spectra of berenil in

Received: May 13, 2020
Published: June 25, 2020



ACS Publications © 2020 American Chemical Society

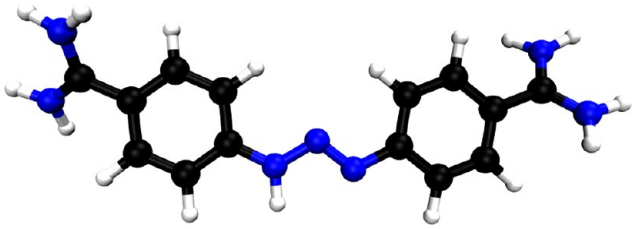


Figure 1. ET conformer of berenil.

solution, in complexation to AT-rich DNA or when bound to trypsin[25] do not show any sign for the persistence of the *E-azo,s-cis* and *Z-azo,s-trans* conformers of berenil under thermodynamically equilibrated conditions.[24] Moreover, ADC(2) calculations and time-resolved spectroscopy indicate that berenil relaxes in a vacuum after photoexcitation on the S_1 surface along a bicycle-pedal pathway. These findings corroborate conclusions drawn from time-resolved fluorescence and transient absorption spectroscopy of berenil in solvents of different viscosities and bound to the DNA minor groove.[24−26]

To gain further insight into the interplay between the nuclear relaxation on the excited-state potential energy surfaces and a confining, rigid environment, we study in this contribution the S_1 relaxation mechanism of berenil in the DNA minor groove with the algebraic diagrammatic construction through second order,[27,28] ADC(2), combined with polarizable embedding,[29] PE-ADC(2). In contrast to conventional QM/MM calculations with point charge embedding, PE-ADC(2) takes the electrostatic response of the environment into account. This is important for a correct description of the solvent (or environment) shift on the excitation energy. In particular, we want to understand here how the DNA environment and solvent molecules couple to the volume-conserving relaxation process of berenil.

2. COMPUTATIONAL DETAILS

2.1. Molecular Dynamics Simulation. The initial structure of berenil in complexation to an AT-rich DNA sequence has been obtained from the X-ray structure (PDB ID: 2GVR).[30] In this X-ray structure, the (ET) conformer of berenil is bound to the minor groove of the DNA. To perform molecular dynamics simulation starting from the X-ray structure, all of the crystallographic water molecules, co-solvents, and counterions were removed, and the berenil molecule was saturated by hydrogen atoms to form a protonated dicationic form. The double protonated dicationic form is the dominant hydrogenation state, under experimental and physiological conditions.[23,31] There are two possibilities for the hydrogen saturation of the central linear triazene functional group of berenil. Since the two tautomeric forms are mirror images, only one of them is considered in this study. The protonation state of DNA was obtained with AmberTools.[32] The DNA-minor-groove-bound structure of berenil, berenil@DNA, has then been solvated in a cubic water box with at least 20 nm distance between the DNA and the box edges. The system was neutralized with Na^+ cations, and then, Na^+ and Cl^- ions were added to reproduce the experimental salt concentration.[25] In the molecular dynamics calculations, the ParmBSC1 parameters[33] of the AMBER force field[34] were used for DNA and the GAFF parameters[35] with MRESP point charges[36] (fitted to the B3LYP/def2-TZVP[37,38] electrostatic potential) were used for berenil. In this simulation, the TIP3P[39] water model was used.

Before proceeding with production-level simulations, a pre-equilibration procedure was carried out. First, the steepest descent minimization for 5000 steps was used to remove unphysical close contacts, followed by NVT molecular dynamics run for 200 ps at T = 300 K with the heavy atoms being restrained. Next, NPT simulation (T = 300 K and P = 1 bar) was carried out, restraining only the heavy atoms of DNA, followed by NPT simulation with no restraints for 200 ps, at T = 300 K and P = 1.0 bar. For the final NVT production run, the box vectors were set based on the averaged values of the previous NPT equilibration run. A 20 ns long NVT production run was then carried out to generate the final trajectory. For all steps, a 2 fs time step was used, and the temperature was controlled by a velocity-rescaling thermostat.[40] The SHAKE[41] algorithm was used to constrain all bonds involving hydrogen atoms. Ten configurations in 2 ns intervals of the trajectory were extracted as a representative set of configurations for generating the embedding potential for the QM/MM calculations. These molecular dynamics calculations were done using GROningen MAchine for Chemical Simulation (GROMACS).[42]

2.2. Calculation of the Polarizable Potential. In this work, we use three embedding models, *vide infra*. In the first two models, the QM subsystems are the berenil molecule while having the DNA (and all water molecules and ions) in the MM subsystems. In the third embedding model, the QM subsystem consists of the berenil molecule and three hydrogen-bonded water molecules, whereas the rest of the system is treated at the MM level. The MM subsystem of the QM/MM calculation is partitioned into three layers. First, a polarizable layer includes the DNA and all water molecules and ions within 5 Å of berenil. This layer used distributed multipoles up to quadrupoles and distributed dipole−dipole polarizabilities. The second layer used static multipole moments up to quadrupoles and comprised the water molecules and ions within 15 Å of berenil. The third layer used point charges and included the remaining water molecules and ions within 30 Å of berenil. A graphical representation of the layered MM subsystem is shown in Figure 2. The polarizabilities and multipole moments

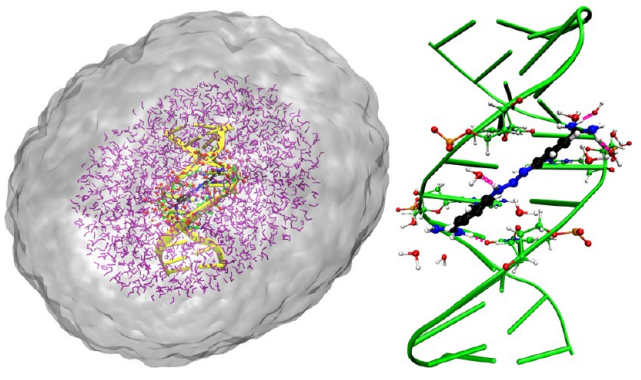


Figure 2. Total system (left) consists of the QM region (berenil) and three MM layers: (i) Polarizable embedding layer including DNA (yellow) and all water molecules and ions within 5 Å of berenil. (ii) Multipole embedding layer including water molecules and ions within 15 Å of berenil (magenta). (iii) Point charge embedding layer including water molecules and ions within 30 Å of berenil (transparent sphere). The polarizable layer of the MM subsystem is shown on the right with atom colors and the DNA sketched in green.

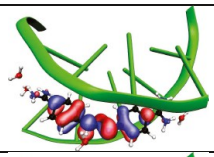
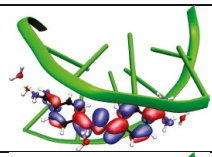
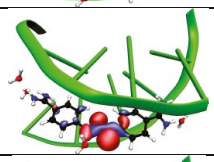
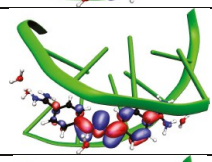
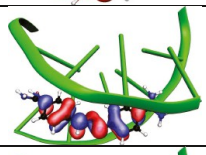
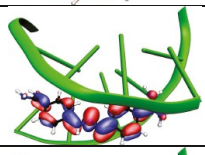
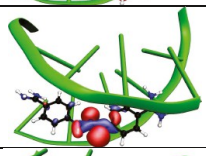
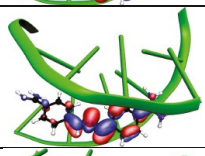
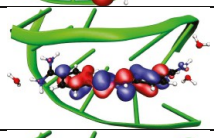
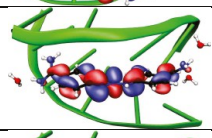
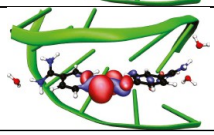
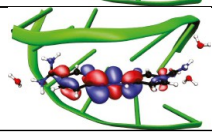
https://dx.doi.org/10.1021/acs.jctc.0c00489
J. Chem. Theory Comput. 2020, 16, 5203−5211

Table 1. Vertical Excitation Energies (ΔE) and Oscillator Strengths (f) of EM1, EM2, and EM3 Models for S_1 and S_2 at the PE(ECP)-ADC(2) Level with SVP and aDZ Basis Sets, on 10 Molecular Configurations that are Extracted from the MD Trajectory[a]

			EM1		EM2		EM3	
level	basis	char.	ΔE (eV)	f	ΔE (eV)	f	ΔE (eV)	f
S_1	aDZ	$\pi\pi^*$	3.03 ± 0.2	1.12 ± 0.2	2.97 ± 0.2	1.14 ± 0.1	3.02 ± 0.2	1.13 ± 0.2
S_1	SVP	$\pi\pi^*$	3.12 ± 0.2	0.94 ± 0.3	3.06 ± 0.2	1.11 ± 0.1	3.11 ± 0.2	0.97 ± 0.3
S_2	aDZ	$n\pi^*$	3.32 ± 0.2	0.13 ± 0.1	3.33 ± 0.2	0.06 ± 0.1	3.30 ± 0.2	0.13 ± 0.1
S_2	SVP	$n\pi^*$	3.34 ± 0.2	0.33 ± 0.3	3.35 ± 0.2	0.11 ± 0.1	3.33 ± 0.2	0.31 ± 0.3

[a]The standard deviations are shown by ±.

Table 2. Vertical Excitation Energies (ΔE) and Oscillator Strengths (f) of EM1, EM2, and EM3 for S_1 and S_2 Electronic States, Calculated at the PE(ECP)-ADC(2)/aDZ Level with PE(ECP)-MP2/SVP Optimized Geometry for EM1, EM2, and EM3[a]

Emb. Model	Char.	ΔE (eV)	f	OCC	VIR
1	$\pi\pi^*$	3.28	1.09		
1	$n\pi^*$	3.58	0.19		
2	$\pi\pi^*$	3.56	1.08		
2	$n\pi^*$	3.99	0.01		
3	$\pi\pi^*$	3.23	1.27		
3	$n\pi^*$	3.60	0.02		

[a]Excitation characters (Char.), first occupied (OCC), and virtual (VIR) pair of NTOS (isosurface ± 0.05) are given.

of DNA have been obtained via the MFCC[43,44] fragmentation procedure, as implemented in the PyFraME package.[45] It employs the Dalton program[46] to calculate distributed multipoles and polarizabilities with the Loprop[47] approach. The polarizabilities and multipoles were calculated at the DFT/B3LYP[37] level with the ANO-recontracted version of the aug-cc-pVDZ basis set.[48,49] For the point charge embedding layer, the solvent embedding potential has been used.[50]

2.3. QM/MM Calculations. The QM/MM excitation energies and oscillator strengths are obtained for 10 configurations, extracted from the molecular dynamics trajectory. The ground- and excited-state geometry optimizations were carried out at the polarizable PE(ECP)-MP2 and PE(ECP)-ADC(2) levels, respectively, with the SVP basis set[51] and the corresponding auxiliary basis set[52] for the resolution-of-the-identity (RI) approximation used in the `ricc2` program.[53] The excitation energies and oscillator strengths have been computed with single-point calculations at the PE(ECP)-ADC(2)/aug-cc-pVDZ[54] (aDZ) level, with the respective optimized auxiliary basis set.[55] The Lennard-Jones parameters for the QM/MM calculations that describe non-electrostatic dispersion and Pauli repulsion interactions between the QM and the MM subsystems are identical to the Lennard-Jones parameters that have been used in the molecular dynamics calculations. All of the atoms of the MM layer that are within 5 Å of berenil were supplemented with polarizabilities as described above and, to avoid electron spill-out, with effective core potentials (ECPs) taken from ref 56. Finally, the results of QM/MM calculations are compared with the vacuum calculations reported in ref 24 and the polarizable

https://dx.doi.org/10.1021/acs.jctc.0c00489
J. Chem. Theory Comput. 2020, 16, 5203−5211

continuum model of aqueous solution (ε = 80.4) at the COSMO-ADC(2)/SVP level of theory. All QM/MM calculations were done with a local development version of the `ricc2` module of the TURBOMOLE program package.[57]

2.4. Models for the Berenil@DNA Complex. To study the confinement effects on excited-state relaxation processes of the berenil@DNA complex, we focused on three models for the embedding environment of berenil. The first embedding model (EM1) serves as an example of the extreme confinement situation. In this model, all of the surrounding molecular environment of berenil has been fixed in space and, thus, the berenil molecule is caged in a fully rigid environment. With this model, we study whether the volume-conserving relaxation motions of berenil can at all be suppressed by DNA-minor-groove confinement and surrounding water molecules, or if the relaxation processes[24,25] for berenil are (almost) completely insensitive to changes in the molecular environment. The effect of DNA embedding alone as confinement on the excited-state relaxation mechanism is investigated with a second embedding model (EM2), where all water molecules and ions from the environment have been removed. A third model (EM3) was used to study the coupling of motions in the first solvation shell to the (excited-state) relaxation in the berenil chromophore. Hydrogen-bond analysis of the production of molecular dynamics trajectory reveals that, effectively, berenil donates 2.5 hydrogen bonds to the surrounding water molecules, cf. Supporting Information. This analysis was performed with the hydrogen-bond analysis tool of the Visual Molecular Dynamics, VMD program.[58] Based on this analysis, for the EM3 model, in addition to berenil, three water molecules that have a hydrogen bond with berenil were included in the flexible QM region, while for the rest of the system, including DNA, other water molecules, and all ions, the positions were fixed in space.

3. RESULTS AND DISCUSSION

In Table 1, the results are listed for the vertical excitation energies and oscillator strengths for the two lowest excited singlet states of berenil obtained with PE(ECP)-ADC(2) in combination with the aDZ or SVP basis sets for 10 molecular configurations and the three models EM1, EM2, and EM3. These 10 geometries are used directly in the QM/MM calculations without further geometry optimization. Compared to the experimental spectrum,[25] the calculated average vertical excitation energies with the models EM1 and EM3 at the PE(ECP)-ADC(2)/aDZ level are red-shifted by ≈0.21 and 0.22 eV, respectively. This is to a certain extent an artifact of using the geometries from the force field calculation in ADC(2), which causes a red shift and increases the standard deviations.[59] However, still, these deviations are close to the error bars of ADC(2).[28,60] The almost perfect agreement between the models EM1 and EM3 (with three water molecules in the QM region) shows that the parameters used in the PE(ECP) calculations are capable of describing the most important interactions between the chromophore and the first solvation shell. The results obtained with the aDZ and the SVP basis sets are in good agreement for both S_1 and S_2 excitation energies. The SVP results are only slightly blue-shifted so that the SVP basis set should be appropriate for studying the relaxation pathways while the results for the oscillator strengths are more sensitive to diffuse functions that are missing in the SVP basis.

The relatively small standard deviations (0.2 eV for $\pi\pi^*$ electronic excitation, Table 1) show that the ground-state dynamics have a marginal effect on the electronic excitations, and thus, it is justified to use a single representative structure for studying the relaxation process. Therefore, we optimized the ground-state geometry of berenil in all three models at the PE(ECP)-MP2/SVP level and then calculated the energy gaps and oscillator strengths with the aDZ basis. In Table 2, the natural transition orbitals (NTOs) for the two lowest excited singlet states of berenil as obtained with PE(ECP)-ADC(2)/aDZ are shown for all three models.[61] The characters of the excited states are the same for all three models. S_1 has $\pi\pi^*$ character, while the second excited singlet state, S_2, shows an $n\pi^*$ transition. In a vacuum, S_2 is a dark state with a very small oscillator strength, due to the approximate planar structure of the molecule. The environment distorts the planarity and induces some oscillator strength for S_2. The effect is larger for models EM1 and EM3 and with the smaller SVP basis. With the more accurate aDZ basis, the oscillator strength of the $n\pi^*$ excitation is about 10 times smaller than that of the $\pi\pi^*$ excitation and, thus, the main relaxation process should occur in the S_1 state. This is in agreement with spectroscopic data[24,25] and complements results on the geometrical dependence of the oscillator strengths.[24]

In comparison to the most stable conformer of berenil in a vacuum, *E-azo-s-trans*,[24] the geometries of berenil do not change substantially with EM1 and EM2 (solvent removed) confinements (Figure 3) and also its almost planar structure is

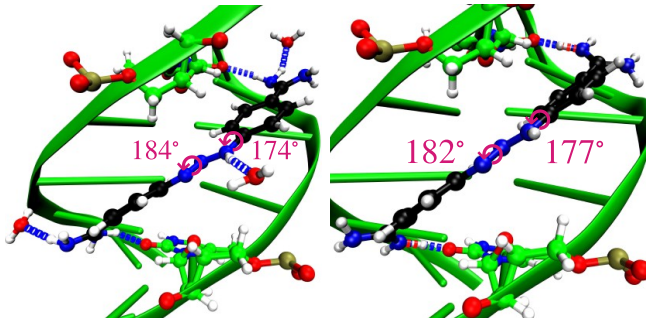


Figure 3. PE-MP2/SVP ground-state relaxed geometries of berenil in the (left) EM1 and (right) EM2.

retained. The minor out-of-plane twist of berenil in the EM1 model is due to interaction with the water network for maximizing the hydrogen-bonding interactions. In model EM1, berenil has five hydrogen bonds with neighboring molecules: two hydrogen bonds with DNA base pairs and three hydrogen bonds with surrounding water molecules. In particular, we observe a hydrogen bond between the hydrogen of the triazene bridge and one of the water molecules of the environment. The excitation energies for the bright $\pi\pi^*$ transition are at 3.28 and 3.23 eV for EM1 and EM3 (the model with three water molecules in the QM region), respectively, which are in excellent agreement with the maximum at 3.24 eV in the experimental berenil@DNA steady-state absorption spectrum. From the comparison between EM3 and EM2, one can identify a 0.33 eV solvatochromic blue shift for EM2, due to the missing interactions with the surrounding water and ions. From the excellent agreement between the results for the full models (EM1 and EM3) and the experiment, and from the similarities between the character of excitations and NTOs, we

https://dx.doi.org/10.1021/acs.jctc.0c00489
J. Chem. Theory Comput. 2020, 16, 5203−5211

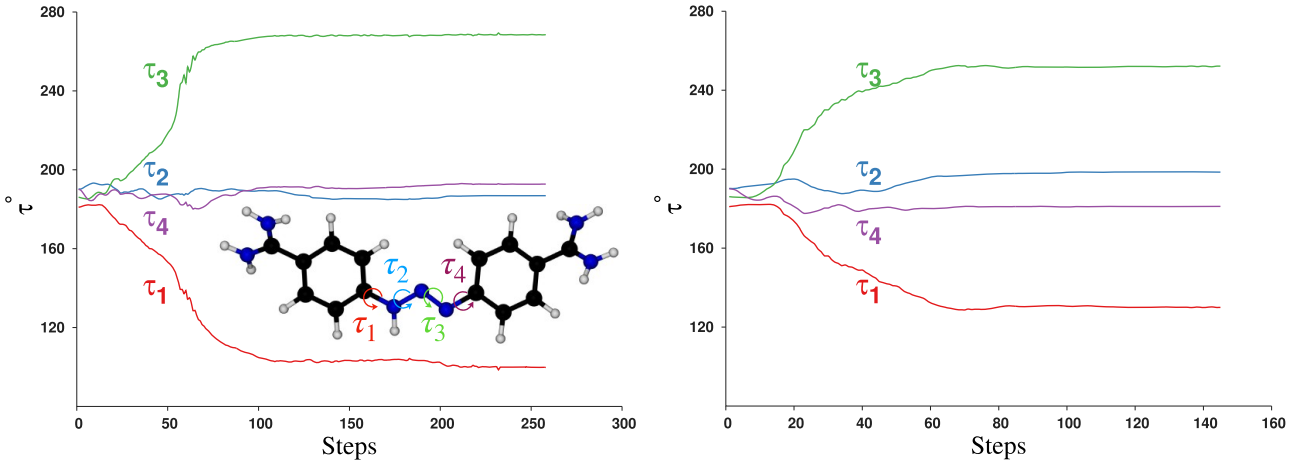


Figure 4. Triazene group torsion angles are given by τ_{1-4}, respectively (cmp. the molecular image on the left panel). The evaluation of the triazene group torsions along the paths from the FC-S_1 geometry of berenil@DNA is shown for (left) EM2 and (right) EM3 calculated at the PE(ECP)-ADC(2)/SVP level of theory. The final structures are given in the Supporting Information.

conclude that our models are capturing the main physics of the vertical $\pi\pi^*$ excitation and thus we can use these models to study the role of confinements in the relaxation processes.

The *in vacuo* deexcitation mechanism on the S_1 potential energy surface of berenil has recently been studied by us with intrinsic reaction coordinate (IRC) calculations.[24] The proposed two-step deexcitation mechanism, first elongation of the N═N bond followed by a volume-conserving bicycle-pedal motion of the triazene group, is in agreement with the time-resolved fluorescence up-conversion measurements of the excited-state deexcitation process in solution and also in the complexation to AT-rich DNA. Figure 4 shows the change of characteristic torsion angles of the triazene group along the paths for the S_1 relaxation process of berenil@DNA for EM2 and EM3. The analysis of the paths for berenil@DNA unveils that bond torsions of the triazene evolve with a mechanism that has predominantly a bicycle-pedal type character, for both EM2 and EM3. In a vacuum, due to the approximate planarity of the ET conformer, the IRC path that starts from the Franck−Condon point on the S_1 surface, FC-S_1, leads to a transition state on the S_1 potential energy surface from where the structure can relax by a forward or a backward bicycle-pedal motion to two similar minima on the S_1 surface.[25]

The optimized S_1 equilibrium structures of berenil@DNA obtained for the two models, EM1 and EM2, are shown in Figure 5. For model EM2 (solvent removed), the angle for the torsion around the N═N azo bond, τ_3, changes during the relaxation from the Franck−Condon point to the S_1 minimum from 182° by 86° to 268° and the angle for the torsion around the phenyl−amino bond τ_1 from 177 to 100°. The S_1 minimum geometry of berenil in the EM2 model is similar to the structure of the S_1 minimum found in a vacuum. Hence, it can be concluded that the berenil S_1 relaxation process is not hindered by DNA confinement.

In contrast, the S_1 equilibrium structure of berenil found with model EM1 (frozen solvent structure) is more different from the S_1 minimum geometry in a vacuum or a polarizable continuum solvation model:[24] the angle for the torsion around the azo bond, τ_3, changed only by 20° from its ground-state value (compared to 92° in vacuum)[24] and the hydrogen bonds that connect berenil to its environment are almost unchanged compared to the ground-state structure.

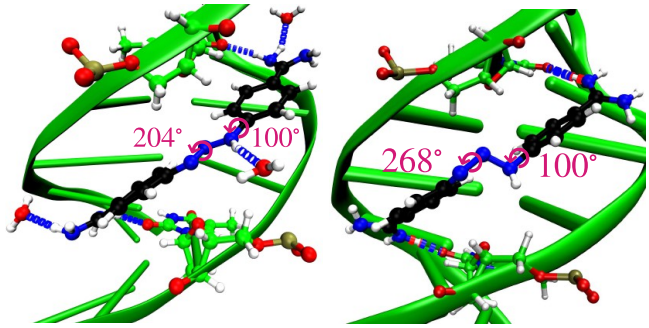


Figure 5. PE(ECP)-ADC(2)/SVP relaxed geometries of berenil in the lowest singlet electronically excited state S_1 within two environment models, EM1 (left) and EM2 (right), cmp. caption of Figure 3.

In Figure 6, the ground- and excited-state equilibrium structures of berenil are compared by superimposing excited- and ground-state structures for the three models, EM1, EM2, and EM3. A comparison between EM2 (middle) and EM3 (right) shows that the S_1 structures are similar for both models. In particular, the internal coordinates of the triazene group are also similar to the vacuum case. Mainly, the torsion angles for the phenyl group differ from the COSMO-ADC(2)/SVP[62] optimized geometry, which are associated with weak force constants, as discussed in ref 24. However, in the model with a fixed water network (EM1), the relaxation is incomplete. As a consequence, the energy gap between S_0 and S_1 at the S_1 equilibrium geometry is with 1.91 eV (≈15 400 cm^{-1}) significantly larger than in a vacuum or with a continuum solvation model for aqueous solution, yielding 0.16 eV (≈1290 cm^{-1}). Thus, for a description of the nonradiative thermal transition to S_0, which is observed in the experiment, it is crucial to include solvent relaxation.

The complete description of the relaxation process requires reorganization of the water molecules in the first solvation shell. In the model EM3, Figure 7, three water molecules that are close to berenil were included in the flexible QM region. The additional flexibility allows the azo-bond N═N torsion angle to change to 252° and reduces the energy gap between S_0 and S_1 at the S_1 equilibrium geometry to 0.42 eV (≈2950 cm^{-1}) in the PE(ECP)-ADC(2)/aDZ calculation (right panel

https://dx.doi.org/10.1021/acs.jctc.0c00489
J. Chem. Theory Comput. 2020, 16, 5203−5211

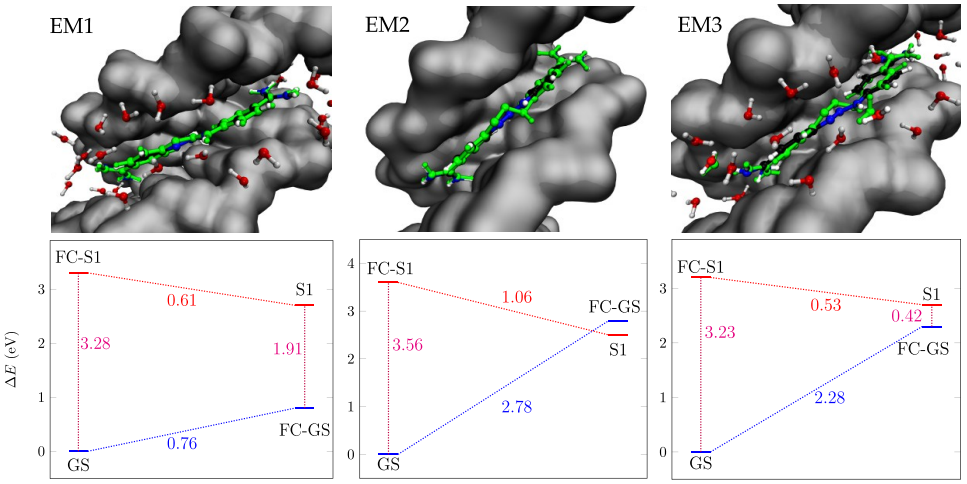


Figure 6. (Top) Ground- and excited-state structures and (down) relaxation paths of berenil@DNA, obtained with the models EM1 (left), EM2 (middle), and EM3 (right) at the PE(ECP)-ADC(2)/aDZ level of theory for the PE(ECP)-ADC(2)/SVP optimized geometries. (Blue) the electronic ground state; (red) the lowest electronic excited state. The geometry of the S_1 equilibrium structure (green) is superimposed on the ground-state geometry (atom colors).

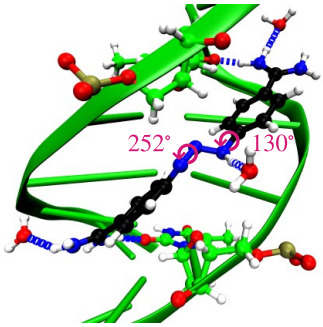


Figure 7. S_1 optimized structure of berenil together with three water molecules for the model EM3 calculated at the QM/MM PE(ECP)-ADC(2)/SVP level of theory. For clarity, MM water molecules and ions are not shown.

in Figure 6), while the hydrogen-bonding interaction between the triazene group and solvent is preserved, cmp. Figure 7. The azo N=N torsion angle at the S_1 minimum differs only by 16° from the value for aqueous solution obtained with COSMO-ADC(2)/SVP. Thus, the excited-state relaxation of berenil@DNA is coupled to the relaxation of the solvation shell. It has been reported that the dynamics of biological and minor-groove water are slower than that of bulk water.[63−68] Together with the above computational results, this explains the prolongation by a factor of approximately 2 of the excited-state lifetime for berenil@DNA compared to berenil in aqueous solution that has been observed in time-resolved fluorescence experiments.[25]

4. CONCLUSIONS

The relaxation of berenil after photoexcitation to S_1 has been studied in the presence of DNA confinement using polarizable QM/MM PE(ECP)-ADC(2) calculations. The same volume-conserving bicycle-pedal type relaxation pathway is found as previously proposed for the gas phase and aqueous solution based on calculations in a vacuum and with a continuum solvation model. To determine the effects of the interactions with the DNA strand and solvent molecules, we used three different computational models. The simplest model, EM2, where the solvent has been replaced by vacuum, shows that the volume-conserving relaxation process found in a vacuum is not hindered by the confinement imposed by the DNA when berenil is bound in the minor groove. The relaxation of berenil on the S_1 surface proceeds to a structure of the triazene group that is similar to the one found in the vacuum and COSMO calculations and, as in the latter case, S_1 and S_0 are energetically very close at the S1 equilibrium structure. The model EM1, with the solvent frozen in the ground-state configuration, was used to study the importance of the relaxation of the solvent configuration for the volume-conserving bicycle-pedal motion of berenil. It showed that the motions in berenil are coupled through the hydrogen bonds to the water molecules in the first solvation shell. Thus, in this extremely confined model with the DNA and the surrounding water molecules being fixed, the relaxation motion of berenil is hindered by the hydrogen-bonded water molecules in the first solvation shell. The most refined model, EM3, with three flexible water molecules in the QM subsystem, includes the most important effects of solvent relaxation. The EM3 model reveals that the volume-conserving bicycle-pedal type relaxation process in berenil is entangled to the relaxation of the first solvation shell via specific intermolecular interactions. It shows that for berenil@DNA, the relaxation of the first solvent shell is needed to reach a region on the S_1 potential energy surface where the energy gap for the de-excitation to the ground state is similarly small as in aqueous solution. This model can explain the nonradiative relaxation of berenil@DNA, and the prolonged excited-state lifetime of berenil@DNA that is observed in time-resolved fluorescence experiments.

■ ASSOCIATED CONTENT

Supporting Information

The Supporting Information is available free of charge at https://pubs.acs.org/doi/10.1021/acs.jctc.0c00489.

Final structures of S_1 relaxation paths for EM2 and EM3 models and hydrogen-bond analysis of the MD trajectory (PDF)

https://dx.doi.org/10.1021/acs.jctc.0c00489
J. Chem. Theory Comput. 2020, 16, 5203−5211

AUTHOR INFORMATION

Corresponding Author

Alireza Marefat Khah − *Quantum Chemistry Group, Ruhr University of Bochum, D-44780 Bochum, Germany;* orcid.org/0000-0002-9593-0344; Email: alireza.marefatkhah@rub.de

Authors

Peter Reinholdt − *Department of Physics, Chemistry and Pharmacy, University of Southern Denmark, 5230 Odense, Denmark;* orcid.org/0000-0003-2406-700X

Patrick Nuernberger − *Institut für Physikalische und Theoretische Chemie, Universität Regensburg, 93040 Regensburg, Germany*

Jacob Kongsted − *Department of Physics, Chemistry and Pharmacy, University of Southern Denmark, 5230 Odense, Denmark;* orcid.org/0000-0002-7725-2164

Christof Hättig − *Quantum Chemistry Group, Ruhr University of Bochum, D-44780 Bochum, Germany;* orcid.org/0000-0002-5752-2710

Complete contact information is available at: https://pubs.acs.org/10.1021/acs.jctc.0c00489

Notes

The authors declare no competing financial interest.

ACKNOWLEDGMENTS

Funded by the Deutsche Forschungsgemeinschaft (DFG, German Research Foundation) under Germany's Excellence Strategy—EXC 2033 — 390677874 — RESOLV. P.R. and J.K. acknowledge the Danish Council for Independent Research for financial support (Grant ID: DFF-7014-00050B). P.N. thanks the DFG for support within the Emmy-Noether program (Grant ID: NU 263/3-1).

ADDITIONAL NOTE

[a]Berenil exhibits three molecular conformers with respect to the triazene NHN═N functional group. In the *E-azo,s-trans* conformer, the azo- N═N double-bond and the NH−N single-bond comprise a trans configuration. The two other conformers, *E-azo,s-cis* and *Z-azo,s-trans*, have a cis configuration around the NH−N single-bond and the N═N double-bond, respectively. The molecular structure of these conformers are given in ref 24.

REFERENCES

(1) Mialocq, J.-C.; Gustavsson, T. *New Trends in Fluorescence Spectroscopy*; Springer: Berlin Heidelberg, 2001; pp 61−80.

(2) Creatini, L.; Cusati, T.; Granucci, G.; Persico, M. Photodynamics of azobenzene in a hindering environment. *Chem. Phys.* **2008**, *347*, 492−502.

(3) Tiberio, G.; Muccioli, L.; Berardi, R.; Zannoni, C. How Does the Trans-Cis Photoisomerization of Azobenzene Take Place in Organic Solvents? *ChemPhysChem* **2010**, *11*, 1018−1028.

(4) Böckmann, M.; Doltsinis, N. L.; Marx, D. Enhanced photoswitching of bridged azobenzene studied by nonadiabatic ab initio simulation. *J. Chem. Phys.* **2012**, *137*, No. 22A505.

(5) Renth, F.; Bahrenburg, J.; Temps, F. *Photon-Working Switches*; Springer: Japan, 2017; pp 237−259.

(6) Nenov, A.; Borrego-Varillas, R.; Oriana, A.; Ganzer, L.; Segatta, F.; Conti, I.; Segarra-Marti, J.; Omachi, J.; Dapor, M.; Taioli, S.; Manzoni, C.; Mukamel, S.; Cerullo, G.; Garavelli, M. UV-Light-Induced Vibrational Coherences: The Key to Understand Kasha Rule Violation in trans-Azobenzene. *J. Phys. Chem. Lett.* **2018**, *9*, 1534−1541.

(7) Tavadze, P.; Avendaño Franco, G.; Ren, P.; Wen, X.; Li, Y.; Lewis, J. P. A Machine-Driven Hunt for Global Reaction Coordinates of Azobenzene Photoisomerization. *J. Am. Chem. Soc.* **2018**, *140*, 285−290.

(8) Boumrifak, C.; Yang, C.; Bellotto, S.; Wegner, H. A.; Wachtveitl, J.; Dreuw, A.; Slavov, C. Isomerization Dynamics of Electronically Coupled but Thermodynamically Decoupled Bisazobenzenes. *ChemPhotoChem* **2019**, *3*, 411−417.

(9) Otolski, C. J.; Mohan Raj, A.; Ramamurthy, V.; Elles, C. G. Ultrafast Dynamics of Encapsulated Molecules Reveals New Insight on the Photoisomerization Mechanism for Azobenzenes. *J. Phys. Chem. Lett.* **2019**, *10*, 121−127.

(10) Conyard, J.; Heisler, I. A.; Chan, Y.; Page, P. C. B.; Meech, S. R.; Blancafort, L. A new twist in the photophysics of the GFP chromophore: a volume-conserving molecular torsion couple. *Chem. Sci.* **2018**, *9*, 1803−1812.

(11) Jung, Y. O.; Lee, J. H.; Kim, J.; Schmidt, M.; Moffat, K.; Šrajer, V.; Ihee, H. Volume-conserving trans−cis isomerization pathways in photoactive yellow protein visualized by picosecond X-ray crystallography. *Nat. Chem.* **2013**, *5*, 212−220.

(12) Pande, K.; Hutchison, C. D. M.; Groenhof, G.; Aquila, A.; Robinson, J. S.; Tenboer, J.; Basu, S.; Boutet, S.; DePonte, D. P.; Liang, M.; White, T. A.; Zatsepin, N. A.; Yefanov, O.; Morozov, D.; Oberthuer, D.; Gati, C.; Subramanian, G.; James, D.; Zhao, Y.; Koralek, J.; Brayshaw, J.; Kupitz, C.; Conrad, C.; Roy-Chowdhury, S.; Coe, J. D.; Metz, M.; Xavier, P. L.; Grant, T. D.; Koglin, J. E.; Ketawala, G.; Fromme, R.; rajer, V.; Henning, R.; Spence, J. C. H.; Ourmazd, A.; Schwander, P.; Weierstall, U.; Frank, M.; Fromme, P.; Barty, A.; Chapman, H. N.; Moffat, K.; van Thor, J. J.; Schmidt, M. Femtosecond structural dynamics drives the trans/cis isomerization in photoactive yellow protein. *Science* **2016**, *352*, 725−729.

(13) Warshel, A. Bicycle-pedal Model for the First Step in the Vision Process. *Nature* **1976**, *260*, 679−683.

(14) Schapiro, I.; Weingart, O.; Buss, V. Bicycle-Pedal Isomerization in a Rhodopsin Chromophore Model. *J. Am. Chem. Soc.* **2009**, *131*, 16−17.

(15) Barbatti, M.; Ruckenbauer, M.; Szymczak, J. J.; Sellner, B.; Vazdar, M.; Antol, I.; Eckert-Maksić, M.; Lischka, H. *Handbook of Computational Chemistry*; Springer International Publishing, 2017; pp 1697−1739.

(16) Liu, R. S. H. Photoisomerization by Hula-Twist: A Fundamental Supramolecular Photochemical Reaction. *Acc. Chem. Res.* **2001**, *34*, 555−562.

(17) Szymczak, J. J.; Barbatti, M.; Lischka, H. Mechanism of Ultrafast Photodecay in Restricted Motions in Protonated Schiff Bases: The Pentadieniminium Cation. *J. Chem. Theory Comput.* **2008**, *4*, 1189−1199.

(18) Cupellini, L.; Calvani, D.; Jacquemin, D.; Mennucci, B. Charge transfer from the carotenoid can quench chlorophyll excitation in antenna complexes of plants. *Nat. Commun.* **2020**, *11*, No. 662.

(19) Loco, D.; Lagardère, L.; Cisneros, G. A.; Scalmani, G.; Frisch, M.; Lipparini, F.; Mennucci, B.; Piquemal, J.-P. Towards large scale hybrid QM/MM dynamics of complex systems with advanced point dipole polarizable embeddings. *Chem. Sci.* **2019**, *10*, 7200−7211.

(20) Waldeck, D. H. Photoisomerization dynamics of stilbenes. *Chem. Rev.* **1991**, *91*, 415−436.

(21) Newton, B. A. *Mechanism of Action of Antimicrobial and Antitumor Agents*;Corcoran, J. W.; Hahn, F. E.; Snell, J. F.; Arora, K. L., Eds.; Springer: Berlin, Heidelberg, 1975; pp 34−47.

(22) Brown, D. G.; Sanderson, M. R.; Skelly, J. V.; Jenkins, T. C.; Brown, T.; Garman, E.; Stuart, D. I.; Neidle, S. Crystal structure of a berenil-dodecanucleotide complex: the role of water in sequence-specific ligand binding. *EMBO J.* **1990**, *9*, 1329−1334.

(23) Reddy, B.; Sondhi, S.; Lown, J. Synthetic DNA minor groove-binding drugs. *Pharmacol. Ther.* **1999**, *84*, 1−111.

(24) Khah, A. M.; Grimmelsmann, L.; Knorr, J.; Nuernberger, P.; Hättig, C. How a linear triazene photoisomerizes in a volume-conserving fashion. *Phys. Chem. Chem. Phys.* **2018**, *20*, 28075−28087.
(25) Grimmelsmann, L.; Khah, A. M.; Spies, C.; Hättig, C.; Nuernberger, P. Ultrafast Dynamics of a Triazene: Excited-State Pathways and the Impact of Binding to the Minor Groove of DNA and Further Biomolecular Systems. *J. Phys. Chem. Lett.* **2017**, *8*, 1986−1992.
(26) Grimmelsmann, L.; Schuabb, V.; Tekin, B.; Winter, R.; Nuernberger, P. Impact of kilobar pressures on ultrafast triazene and thiacyanine photodynamics. *Phys. Chem. Chem. Phys.* **2018**, *20*, 18169−18175.
(27) Schirmer, J. Beyond the random-phase approximation: A new approximation scheme for the polarization propagator. *Phys. Rev. A* **1982**, *26*, 2395−2416.
(28) Hättig, C. Structure optimizations for excited states with correlated second-order methods: CC2, CIS(D∞), and ADC(2). *Adv. Quantum Chem.* **2005**, *50*, 37−60.
(29) Marefat Khah, A.; Khani, S. K.; Hättig, C. Analytic Excited State Gradients for the QM/MM Polarizable Embedded Second-Order Algebraic Diagrammatic Construction for the Polarization Propagator PE-ADC(2). *J. Chem. Theory Comput.* **2018**, *14*, 4640−4650.
(30) Lee, M.; Parkinson, G.; Neidle, S. Crystal structure of the berenil-D(CGCGAATTCGCG)2complex at 1.65 A resolution. https://doi.org/10.2210/pdb2gvr/pdb2007.
(31) Zsila, F. Glycosaminoglycans are potential pharmacological targets for classic DNA minor groove binder drugs berenil and pentamidine. *Phys. Chem. Chem. Phys.* **2015**, *17*, 24560−24565.
(32) Salomon-Ferrer, R.; Case, D. A.; Walker, R. C. An overview of the Amber biomolecular simulation package. *Wiley Interdiscip. Rev.: Comput. Mol. Sci.* **2013**, *3*, 198−210.
(33) Ivani, I.; Dans, P. D.; Noy, A.; Pérez, A.; Faustino, I.; Hospital, A.; Walther, J.; Andrio, P.; Goñi, R.; Balaceanu, A.; Portella, G.; Battistini, F.; Gelpí, J. L.; González, C.; Vendruscolo, M.; Laughton, C. A.; Harris, S. A.; Case, D. A.; Orozco, M. Parmbsc1: a refined force field for DNA simulations. *Nat. Methods* **2015**, *13*, 55−58.
(34) Cornell, W. D.; Cieplak, P.; Bayly, C. I.; Gould, I. R.; Merz, K. M.; Ferguson, D. M.; Spellmeyer, D. C.; Fox, T.; Caldwell, J. W.; Kollman, P. A. A second generation force field for the simulation of proteins, nucleic acids, and organic molecules. *J. Am. Chem. Soc.* **1995**, *117*, 5179−5197.
(35) Wang, J.; Wang, W.; Kollman, P. A.; Case, D. A. Automatic atom type and bond type perception in molecular mechanical calculations. *J. Mol. Graphics Modell.* **2006**, *25*, 247−260.
(36) Bayly, C. I.; Cieplak, P.; Cornell, W. D.; Kollman, P. A. A Well-Behaved Electrostatic Potential Based Method Using Charge Restraints for Deriving Atomic Charges: The RESP Model. *J. Phys. Chem. A* **1993**, *97*, 10269−10280.
(37) Becke, A. D. Density-Functional exchange-energy approximation with correct asymptotic behavior. *Phys. Rev. A* **1988**, *38*, 3098−3100.
(38) Weigend, F.; Ahlrichs, R. Balanced basis sets of split valence, triple zeta valence and quadruple zeta valence quality for H to Rn: Design and assessment of accuracy. *Phys. Chem. Chem. Phys.* **2005**, *7*, 3297−3305.
(39) Jorgensen, W. L.; Chandrasekhar, J.; Madura, J. D.; Impey, R. W.; Klein, M. L. Comparison of Simple Potential Functions for Simulating Liquid Water. *J. Chem. Phys.* **1983**, *79*, 926−935.
(40) Bussi, G.; Donadio, D.; Parrinello, M. Canonical sampling through velocity rescaling. *J. Chem. Phys.* **2007**, *126*, No. 014101.
(41) Ryckaert, J.-P.; Ciccotti, G.; Berendsen, H. J. Numerical integration of the cartesian equations of motion of a system with constraints: molecular dynamics of n-alkanes. *J. Comput. Phys.* **1977**, *23*, 327−341.
(42) Abraham, M. J.; Murtola, T.; Schulz, R.; Páll, S.; Smith, J. C.; Hess, B.; Lindahl, E. GROMACS: High performance molecular simulations through multi-level parallelism from laptops to supercomputers. *SoftwareX* **2015**, *1−2*, 19−25.
(43) He, X.; Zhang, J. Z. H. A new method for direct calculation of total energy of protein. *J. Chem. Phys.* **2005**, *122*, No. 031103.
(44) Söderhjelm, P.; Aquilante, F.; Ryde, U. Calculation of Protein-Ligand Interaction Energies by a Fragmentation Approach Combining High-Level Quantum Chemistry with Classical Many-Body Effects. *J. Phys. Chem. B* **2009**, *113*, 11085−11094.
(45) Olsen, J. M. H. *Pyframe: Python Tools For Fragment-Based Multiscale Embedding*, 2018.
(46) Aidas, K.; Angeli, C.; Bak, K. L.; Bakken, V.; Bast, R.; Boman, L.; Christiansen, O.; Cimiraglia, R.; Coriani, S.; Dahle, P.; Dalskov, E. K.; Ekström, U.; Enevoldsen, T.; Eriksen, J. J.; Ettenhuber, P.; Fernández, B.; Ferrighi, L.; Fliegl, H.; Frediani, L.; Hald, K.; Halkier, A.; Hättig, C.; Heiberg, H.; Helgaker, T.; Hennum, A. C.; Hettema, H.; Hjertenæs, E.; Høst, S.; Høyvik, I.-M.; Iozzi, M. F.; Jansik, B.; Jensen, H. J. A.; Jonsson, D.; Jørgensen, P.; Kauczor, J.; Kirpekar, S.; Kjærgaard, T.; Klopper, W.; Knecht, S.; Kobayashi, R.; Koch, H.; Kongsted, J.; Krapp, A.; Kristensen, K.; Ligabue, A.; Lutnæs, O. B.; Melo, J. I.; Mikkelsen, K. V.; Myhre, R. H.; Neiss, C.; Nielsen, C. B.; Norman, P.; Olsen, J.; Olsen, J. M. H.; Osted, A.; Packer, M. J.; Pawlowski, F.; Pedersen, T. B.; Provasi, P. F.; Reine, S.; Rinkevicius, Z.; Ruden, T. A.; Ruud, K.; Rybkin, V. V.; Salek, P.; Samson, C. C. M.; de Merás, A. S.; Saue, T.; Sauer, S. P. A.; Schimmelpfennig, B.; Sneskov, K.; Steindal, A. H.; Sylvester-Hvid, K. O.; Taylor, P. R.; Teale, A. M.; Tellgren, E. I.; Tew, D. P.; Thorvaldsen, A. J.; Thøgersen, L.; Vahtras, O.; Watson, M. A.; Wilson, D. J. D.; Ziolkowski, M.; Ågren, H. The Dalton Quantum Chemistry Program System. *Wiley Interdiscip. Rev.: Comput. Mol. Sci.* **2014**, *4*, 269.
(47) Gagliardi, L.; Lindh, R.; Karlström, G. Local Properties of Quantum Chemical Systems: The LoProp Approach. *J. Chem. Phys.* **2004**, *121*, 4494−4500.
(48) Söderhjelm, P.; Krogh, J. W.; Karlström, G.; Ryde, U.; Lindh, R. Accuracy of distributed multipoles and polarizabilities: Comparison between the LoProp and MpProp models. *J. Comput. Chem.* **2007**, *28*, 1083−1090.
(49) Schwabe, T.; Olsen, J. M. H.; Sneskov, K.; Kongsted, J.; Christiansen, O. Solvation Effects on Electronic Transitions: Exploring the Performance of Advanced Solvent Potentials in Polarizable Embedding Calculations. *J. Chem. Theory Comput.* **2011**, *7*, 2209−2217.
(50) Boulanger, E.; Thiel, W. Toward QM/MM Simulation of Enzymatic Reactions with the Drude Oscillator Polarizable Force Field. *J. Chem. Theory Comput.* **2014**, *10*, 1795−1809.
(51) Schäfer, A.; Horn, H.; Ahlrichs, R. Fully optimized contracted Gaussian basis sets for atoms Li to Kr. *J. Chem. Phys.* **1992**, *97*, 2571−2577.
(52) Weigend, F.; Häser, M.; Patzelt, H.; Ahlrichs, R. RI-MP2: optimized auxiliary basis sets and demonstration of efficiency. *Chem. Phys. Lett.* **1998**, *294*, 143−152.
(53) Hättig, C.; Weigend, F. CC2 excitation energy calculations on large molecules using the resolution of the identity approximation. *J. Chem. Phys.* **2000**, *113*, 5154−5161.
(54) Kendall, R. A.; Dunning, T. H.; Harrison, R. J. Electron affinities of the first-row atoms revisited. Systematic basis sets and wave functions. *J. Chem. Phys.* **1992**, *96*, 6796−6806.
(55) Weigend, F.; Köhn, A.; Hättig, C. Efficient use of the correlation consistent basis sets in resolution of the identity MP2 calculations. *J. Chem. Phys.* **2002**, *116*, 3175−3183.
(56) Marefat Khah, A.; Reinholdt, P.; Olsen, J. M. H.; Kongsted, J.; Hättig, C. Avoiding Electron Spill-Out in QM/MM Calculations on Excited States with Simple Pseudopotentials. *J. Chem. Theory Comput.* **2020**, *16*, 1373−1381.
(57) *TURBOMOLE*, V7.3 2018 and V7.4 2019, Karlsruhe GmbH, 1989-2007, TURBOMOLE GmbH; University of Karlsruhe and Forschungszentrum, 2007.
(58) Humphrey, W.; Dalke, A.; Schulten, K.; et al. VMD: visual molecular dynamics. *J. Mol. Graphics* **1996**, *14*, 33−38.
(59) Kjellgren, E. R.; Olsen, J. M. H.; Kongsted, J. Importance of Accurate Structures for Quantum Chemistry Embedding Methods:

Which Strategy Is Better? *J. Chem. Theory Comput.* **2018**, *14*, 4309−4319.
(60) Loos, P.-F.; Jacquemin, D. Is ADC(3) as Accurate as CC3 for Valence and Rydberg Transition Energies. *J. Phys. Chem. Lett.* **2020**, *11*, 974−980.
(61) Dunning, T. H., Jr. Gaussian basis sets for use in correlated molecular calculations. I. The atoms boron through neon and hydrogen. *J. Chem. Phys.* **1989**, *90*, 1007−1023.
(62) Khani, S. K.; Khah, A. M.; Hättig, C. COSMO-RI-ADC(2) excitation energies and excited state gradients. *Phys. Chem. Chem. Phys.* **2018**, *20*, 16354−16363.
(63) Pal, S. K.; Peon, J.; Zewail, A. H. Biological water at the protein surface: Dynamical solvation probed directly with femtosecond resolution. *Proc. Natl. Acad. Sci. U.S.A.* **2002**, *99*, 1763−1768.
(64) Pal, S. K.; Zhao, L.; Zewail, A. H. Water at DNA surfaces: Ultrafast dynamics in minor groove recognition. *Proc. Natl. Acad. Sci. U.S.A.* **2003**, *100*, 8113−8118.
(65) Pal, S. K.; Zhao, L.; Xia, T.; Zewail, A. H. Site- and sequence-selective ultrafast hydration of DNA. *Proc. Natl. Acad. Sci. U.S.A.* **2003**, *100*, 13746−13751.
(66) Sen, S.; Andreatta, D.; Ponomarev, S. Y.; Beveridge, D. L.; Berg, M. A. Dynamics of Water and Ions Near DNA: Comparison of Simulation to Time-Resolved Stokes-Shift Experiments. *J. Am. Chem. Soc.* **2009**, *131*, 1724−1735.
(67) Grossman, M.; Born, B.; Heyden, M.; Tworowski, D.; Fields, G. B.; Sagi, I.; Havenith, M. Correlated structural kinetics and retarded solvent dynamics at the metalloprotease active site. *Nat. Struct. Mol. Biol.* **2011**, *18*, 1102−1108.
(68) Laage, D.; Elsaesser, T.; Hynes, J. T. Water Dynamics in the Hydration Shells of Biomolecules. *Chem. Rev.* **2017**, *117*, 10694−10725.

https://dx.doi.org/10.1021/acs.jctc.0c00489
J. Chem. Theory Comput. 2020, 16, 5203−5211